Optics Letters

On the importance of electron impact processes in excimer-pumped alkali laser-induced plasmas

Aram H. Markosyan[1,2]

[1]Department of Electrical Engineering and Computer Science, University of Michigan, Ann Arbor, Michigan 48109-2122, USA
[2]Sandia National Laboratories, Scalable Modeling & Analysis, Livermore, California 94550, USA (amarkos@sandia.gov)

Received 13 September 2017; accepted 21 September 2017; posted 25 September 2017 (Doc. ID 307061); published 18 October 2017

The excimer-pumped alkali laser (XPAL) system has recently been demonstrated in several different mixtures of alkali vapor and rare gas. Without special preventive measures, plasma formation during operation of XPAL is unavoidable. Recent advancements in the availability of reliable data for electron impact collisions with atoms and molecules have enabled development of a complete reaction mechanism to investigate XPAL-induced plasmas. We report on pathways leading to plasma formation in an $Ar/C_2H_6/Cs$ XPAL sustained at different cell temperatures. We find that depending on the operating conditions, the contribution of electron impact processes can be as little as bringing the excitation of $Cs(^2P)$ states to higher level Cs states, and can be as high as bringing $Cs(^2P)$ excited states to a full ionization. Increasing the input pumping power or cell temperature, or decreasing the C_2H_6 mole fraction leads to electron impact processes dominating in plasma formation over the energy pooling mechanisms previously reported in literature.**

OCIS codes: (140.2180) Excimer lasers; (140.5560) Pumping; (140.2020) Diode lasers; (020.5780) Rydberg states; (260.3230) Ionization; (350.5400) Plasmas.

https://doi.org/10.1364/OL.42.004295

Diode-pumped alkali lasers (DPALs) [1–3] and excimer-pumped [4–7] alkali lasers (XPALs) have been extensively studied since their first demonstration. DPALs operate on the $D_1(6^2P_{1/2} \rightarrow 6^2S_{1/2})$ transition of the alkali atom, pumped via optical absorption of the pump radiation on the $D_2(6^2S_{1/2} \rightarrow 6^2P_{3/2})$ transition, followed by fast collisional relaxation to the upper laser level $6^2P_{1/2}$. This system enables the use of high-power semiconductor laser diodes as the pump source to pump a gas laser and efficiently convert the low-brightness diode laser photons into a high-brightness atomic laser beam. One disadvantage of DPALs is that pumping requires a spectrally narrow (≈10 GHz) bandwidth. This means that only a limited potion of the semiconductor laser power will be absorbed, as semiconductor lasers typically emit with bandwidths larger than 100 GHz. To address this weakness, an XPAL photo association of alkali–rare-gas atomic collision pairs provides an alternative approach to DPALs. In XPAL, CsAr $(B^2\Sigma^+_{1/2})$ is optically pumped by 837 nm pulses, followed by its dissociation and production of $Cs(6^2P_{3/2})$. Lasing can occur on both D_1 and D_2 transition lines.

During operation of DPAL [8,9] and XPAL [10], high densities of plasmas are potentially formed. The plasma formation can be more of an issue for XPAL due to higher pump intensities. Along with plasma formation, heating of the gas also occurs. While various studies have proposed different cooling mechanisms [1,11–13], the lack of high-fidelity cross-section data made the plasma formation study limited. In this work, we fill this gap and investigate the importance of electron impact processes in the plasma formation during operation of XPAL. The computational model used in this investigation is global-kin, a first-principles global plasma kinetics model described in detail in Ref. [14]. The model includes calculation of rate equations for species densities, temperatures, pump intensities, and laser intensities that are integrated as a function of time over successive laser pulses and interpulse periods. Electron impact processes are included in global-kin for elastic and inelastic collisions, including electronic and vibrational excitations, super-elastic collisions, ionization, and recombination. The coefficients for electron impact processes are obtained from solutions of Boltzmann's equation for the electron energy distribution function and are functions of electron temperature, which comes from solution of the electron energy conservation equation.

The gas mixture of $Ar/C_2H_6/Cs$ at 600 Torr pressure sustained in a cell at temperatures of 425–490 K, which was experimentally investigated in Ref. [4]. In this investigation, we varied the mole fraction of ethane from 1% to 20%. Our results are insensitive to the choice of the initial condition of electron density, which has a value of 10^6 cm^{-3} in our model. The initial Cs/Cs_2 densities are calculated by the vapor pressure based on the temperature of the laser cell. The cell used in this computational study is described in Refs. [5,10], which is a 5 cm long resonator with a rear mirror having 100% reflectivity and the output coupler with 98% reflectivity for the laser wavelength. The XPAL is pumped longitudinally with a single pass of the pump beam.

The reaction mechanism developed in this study considers 629 reactions among the following species: e, $Cs(6^2S_{1/2},$

$6^2P_{1/2}$, $6^2P_{3/2}$, $5^2D_{3/2}$, $5^2D_{5/2}$, $7^2S_{1/2}$, $7^2P_{1/2}$, $7^2P_{3/2}$, Ryd), Cs^+, Cs_2, Cs_2^+, Cs_2^*, Ar, Ar_2^*, Ar^+, Ar_2^+, Ar($1s_5$, $1s_4$, $1s_3$, $1s_2$, 4p, 4d), CsAr(A $^2\Pi_{1/2}$, A $^2\Pi_{3/2}$, B $^2\Sigma_{1/2}^+$), $CsAr^+$(X, A), C_2H_6, C_2H_6(v13, v24), $C_2H_6^+$. Optical intensities include the laser pump intensity, φ_p, and laser intensities for the Cs ($6^2P_{1/2}$)→ Cs($6^2S_{1/2}$) transition, φ_1(894.59 nm), and the Cs($6^2P_{3/2}$)→ Cs($6^2S_{1/2}$) transition, φ_2(852.35 nm). Our model includes all electron impact processes with Cs, Ar, and C_2H_6. The electron impact cross sections for Cs were calculated using fully relativistic all-electron B-spline R-matrix (BSR) with pseudo-states ansatz with 311 coupled states [5].

We investigated the dominant reaction pathways leading to generation or loss of the species of interest using the open-source package PumpKin [15,16]. PumpKin is a post-processing software that aids in identifying mechanisms by combining elementary reactions that produce and consume the short-lifetime (fast) species into reactive pathways.

In the demonstration XPAL system, pump radiation propagates through a quartz cell heated to 450 K containing 600 Torr of $Ar/C_2H_6/Cs = 98/2/5.7 \times 10^{-5}$. The pump pulses at 837 nm are 5 ns at 1 MHz pulse repetition frequency with a power of 60 MW/cm^2. In Fig. 1, we show the densities of Cs species along with the electron density during the 40th pulse. The XPAL operates by optically pumping CsAr($B^2\Sigma_{1/2}^+$) using 837 nm pulses, followed by the dissociation of CsAr ($B^2\Sigma_{1/2}^+$) and population of the Cs($6^2P_{3/2}$) state. The Cs ($6^2P_{3/2}$) state is further collisionally quenched by ethane to the Cs($6^2P_{1/2}$) state. Furthermore, lasing can occur on both Cs($6^2P_{3/2}$)→ Cs($6^2S_{1/2}$) (852.35 nm) and Cs($6^2P_{1/2}$)→ Cs ($6^2S_{1/2}$) (894.59 nm) transitions. Electron density builds up on a pulse-to-pulse basis and within a few pulses reaches pulse-periodic steady state values of 1.3×10^{13} cm^{-3}.

The following discussion traces the origin of plasma formation. Once the Cs(6^2P) states are formed, following relaxation of CsAr($B^2\Sigma_{1/2}^+$), the energy pooling between these states populates Cs(7P) and Rydberg states [17]:

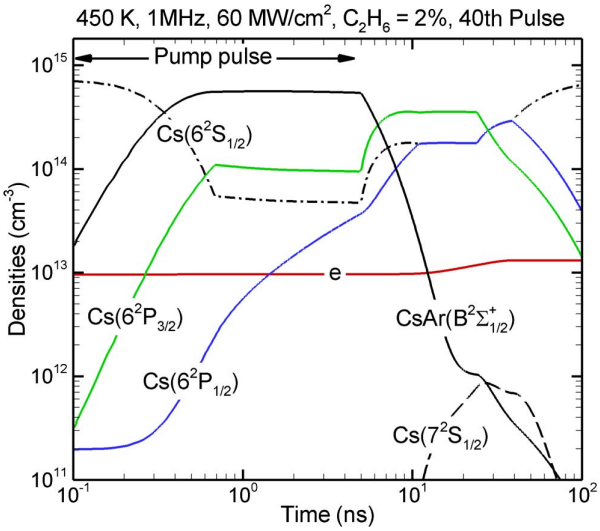

Fig. 1. Densities of cesium species and the electron density as a function of time for XPAL in the mixture of $Ar/C_2H_6/Cs = 98/2/5.7 \times 10^{-5}$ sustained in the cell at 450 K and pumped at 1 MHz with 60 MW/cm^2 power density.

$$Cs(6^2P_{1/2}) + Cs(6^2P_{1/2}) \rightarrow Cs + Cs(7^2P_{1/2,3/2}), \quad (1)$$

$$Cs(6^2P_{3/2}) + Cs(6^2P_{3/2}) \rightarrow Cs + Cs(Ryd), \quad (2)$$

where the rate coefficients for $T_{gas} = 450$ K are, respectively, 7×10^{-10} cm^{-3} s^{-1} and 1×10^{-10} cm^{-3} s^{-1}. Excited states of Cs(6^2P) can be depleted by electron impact processes [$e_{hot} + Cs^* \rightarrow Cs^{**} + e_{cold}$], and electron impact superelastic reactions [$e_{cold} + Cs^{**} \rightarrow Cs^* + e_{hot}$] can repopulate Cs($6^2P$) states [5]. The 7S, 7P, and Rydberg states are photoionized by the φ_1, φ_2, or φ_p photons [11]:

$$\varphi_{1,2,p} + Cs(7^2S, 7^2P, Ryd) \rightarrow Cs^+ + e, \quad (3)$$

where the rate coefficient is 6×10^{-7} cm^{-3} s^{-1}. During laser oscillation, the Cs(6^2P) and Cs(6^2S) states are saturated by the intracavity intensity.

When the 7P states are populated by energy-pooling collisions leading to ionization or formation of higher excited states that can be photoionized by $\varphi_{1,2,p}$, we refer to this mechanism as the *energy pooling mechanism*. When the excitation of 7P states result from electron impact collisions leading to ionization (either stepwise or Penning) or formation of higher excited states that are then photoionized by $\varphi_{1,2,p}$, we refer to this mechanism as the *electron impact mechanism*.

During the first pump pulse, 90% of plasma is formed by the energy-pooling mechanism in which the energy pooling populates the 7S, 7P, and Rydberg states, and photoionization by φ_1 (55%), φ_2 (40%), and φ_p (5%) photons produces the plasma. Less than 10% of the plasma is formed by the electron impact mechanism in which the electron impact excitation populates 7S, and photoionization by φ_1 produces the plasma:

$$e + Cs(6^2P_{3/2}) \rightarrow Cs(7^2S_{1/2}) + e, \quad (4)$$

$$\varphi_1 + Cs(7^2S_{1/2}) \rightarrow Cs^+ + e. \quad (5)$$

After a few pump pulses, the electron density increases and reaches a pulse-periodic steady-state value of 1.3×10^{13} cm^{-3}. At this point, the energy-pooling mechanism is responsible for only 33% of the ionization, while electron impact contributes up to 55% of plasma formation. The remaining plasma is forming by the combination of both mechanisms:

$$Cs(6^2P_{1/2}) + Cs(6^2P_{1/2}) \rightarrow Cs + Cs(7^2P_{3/2}), \quad (6)$$

$$e + Cs(7^2P_{3/2}) \rightarrow Cs(Ryd) + e, \quad (7)$$

$$\varphi_{1,2} + Cs(Ryd) \rightarrow Cs^+ + e. \quad (8)$$

We will refer to the latter mechanism as *mixed mechanism*. In the pulse-periodic steady state, 51% of photoionization is produced by φ_1 photons, while 40% is produced by φ_2. The photoionization produced by the pump radiation produces less than 10% of the plasma.

The cross sections for the electron impact processes with Cs are very large, producing rate coefficients for electron temperatures of less than 0.1 eV on the order of 10^{-8} to 10^{-6} cm^3 s^{-1}. Once the energy-pooling mechanism generates enough electrons, electrons will be heated in superelastic collisions. When the electron temperature is high enough and/or when electron density is high enough, the electron impact mechanism dominates over the energy-pooling mechanism.

The importance of the electron impact mechanism is highly sensitive to the mole fraction of ethane. Babaeva *et al.* [5] showed that for high values of the mole fraction of the

collisional relaxant (nitrogen in Ref. [5]), more than 40%, the lasing occurs on the $Cs(6^2P_{1/2}) \rightarrow Cs(6^2S_{1/2})$ (894.59 nm) transition, while for lower mole fractions, less than 0.35%, the lasing is primarily on the $Cs(6^2P_{3/2}) \rightarrow Cs(6^2S_{1/2})$ (852.35 nm) transition line. The trends hold for the XPAL with ethane as the relaxant agent. The important contributions of the three ionization mechanisms and the fractional ionization ([e]/[Cs] × 100%) as a function of ethane mole fraction are shown in Fig. 2. The cell temperature and pump pulse frequency, as well as power, are the same as discussed above. Lowering the mole fraction of ethane increases the mole fraction of argon, which produces better absorption of the pump power [φ_p(837 nm) + $Cs(6^2S_{1/2})$ + Ar → $CsAr(B\ ^2\Sigma^+_{1/2})$], which, through the processes discussed above, increases the fractional ionization and makes an electron impact a dominant mechanism for formation of the plasma. In this regime, due to insufficient relaxation of $Cs(6^2P_{3/2}) \rightarrow Cs(6^2P_{1/2})$, the lasing is primarily on the 852 nm transition. On the other hand, the higher mole fractions of ethane, the higher the collisional relaxation for $Cs(6^2P_{3/2})$ state, which produces lasing on 894 nm transition line. In such a regime, when the electron density is lower, the energy-pooling mechanism dominates.

The contributions of the electron impact (solid lines) and the mixed (dashed lines) mechanisms for 1%, 2%, and 3% mole fractions of ethane are shown in Fig. 3 as a function input pump power. Lasing starts when pumping power is higher than 6–8 MW/cm^2. Therefore, for lower input power's ionization is due to the pump radiation and the electron impact mechanism in the following:

$$e + Cs(6^2P_{3/2}) \rightarrow Cs(7^2S_{1/2}) + e, \quad \textbf{(9)}$$

$$e + Cs(7^2S_{1/2}) \rightarrow Cs(7^2P_{3/2}) + e, \quad \textbf{(10)}$$

$$\varphi_p + Cs(7^2P_{3/2}) \rightarrow Cs^+ + e. \quad \textbf{(11)}$$

When increasing pump powers, the laser intensities, electron densities, and, hence, the plasma formation mechanisms

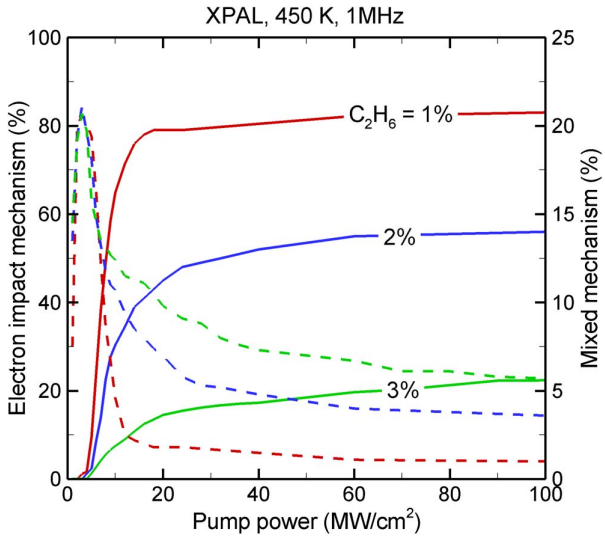

Fig. 3. Importance of the electron impact (left axis, solid lines) and mixed (right axis, dashed lines) mechanisms in plasma formation as a function of input pump power for the ethane mole fractions of 1% (red), 2% (blue), and 3% (green). XPAL is sustained in the cell at 450 K and pumped at 1 MHz frequency.

saturate. The higher the mole fraction of ethane, the higher the electron density, which means the contributions of electron impact processes are increased.

The importance of mechanisms in the plasma formation and fractional ionization as a function of cell temperature are shown in Fig. 4 for XPAL with a pumping power of 60 MW/cm^2 and 2% of ethane. With the increase of cell temperature, the cesium vapor density is increased. Since the pumping power is high enough to achieve oscillation for all temperatures, the fractional ionization increases as well. For the lower temperatures, energy pooling dominates due to

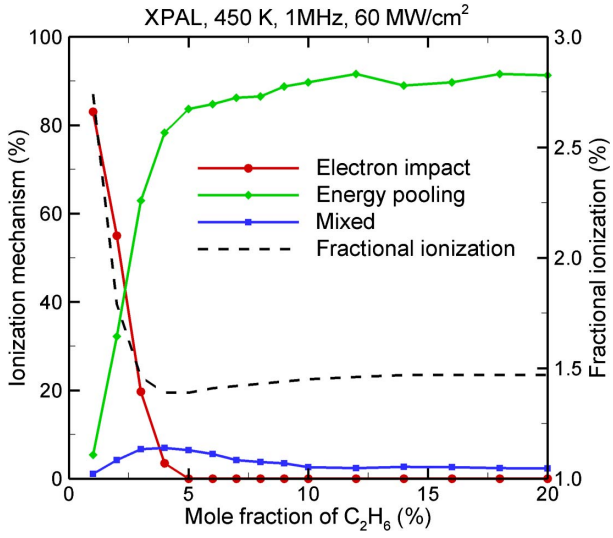

Fig. 2. Contributions of different mechanisms of plasma formation (left axis, solid lines) and the fractional ionization (right axis, dashed line) as a function of the mole fraction of ethane for the XPAL sustained in the cell at 450 K and pumped at 1 MHz with 60 MW/cm^2 power density.

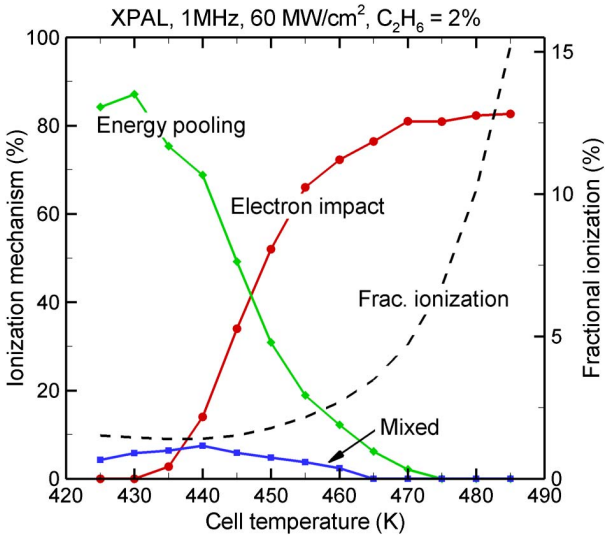

Fig. 4. Contributions of different mechanisms of plasma formation (solid lines) and the fractional ionization (dashed line) as a function of the cell temperature for the XPAL pumped at 1 MHz with pumping power density of 60 MW/cm^2. The mole fraction of ethane is 2%.

the low electron densities. Increasing cell temperature increases the electron density (and the electron temperature, which increases from 0.2 eV for 450 K to 0.7 eV for 500 K) and the importance of electron impact processes. For higher cell temperatures, plasma formation is due to photoionization of 7S, 7P, and Rydberg states and the electron impact multistep ionization process shown below:

$$e + Cs(6^2P_{3/2}) \rightarrow Cs(7^2S_{1/2}) + e, \quad (12)$$

$$e + Cs(7^2S_{1/2}) \rightarrow Cs(7^2P_{1/2,3/2}) + e, \quad (13)$$

$$e + Cs(7^2P_{1/2,3/2}) \rightarrow Cs(Ryd) + e, \quad (14)$$

$$e + Cs(Ryd) \rightarrow Cs^+ + e + e. \quad (15)$$

In conclusion, the recent advances in high-fidelity data for the electron impact processes enabled self-consistent modeling of XPALs sustained in cesium. We find that the electron impact processes play a crucial role in the operation of XPAL and XPAL-formed plasma. Electron impact processes dominate when the cell temperature and/or pumping power are high, and/or when the mole fraction of the collisional relaxant is low. This understanding of underlying fundamental processes can help in preventing an unfavorable plasma formation and increase the efficiency of the overall system.

Funding. U.S. Department of Defense (DOD) High Energy Laser Multidisciplinary Research Initiative (DE-NA0003525).

Acknowledgment. We thank Professor Mark J. Kushner for valuable discussions. Sandia National Laboratories is a multimission laboratory managed and operated by National Technology and Engineering Solutions of Sandia, LLC, a wholly owned subsidiary of Honeywell International, Inc., for the U.S. Department of Energy's National Nuclear Security Administration.

REFERENCES

1. W. F. Krupke, Prog. Quantum Electron. **36**, 4 (2012).
2. B. V. Zhdanov and R. J. Knize, Opt. Eng. **52**, 021010 (2012).
3. F. Gao, F. Chen, J. Xie, D. Li, L. Zhang, G. Yang, J. Guo, and L. Guo, Optik **124**, 4353 (2013).
4. J. D. Readle, C. J. Wagner, J. T. Verdeyen, T. M. Spinka, D. L. Carroll, and J. G. Eden, Proc. SPIE **7581**, 75810K (2010).
5. N. Y. Babaeva, O. Zatsarinny, K. Bartschat, and M. J. Kushner, Proc. SPIE **8962**, 89620D (2014).
6. J. D. Readle, C. J. Wagner, J. T. Verdeyen, D. L. Carroll, and J. G. Eden, Proc. SPIE **7196**, 71960D (2009).
7. A. D. Palla, J. T. Verdeyen, and D. L. Carroll, Proc. SPIE **7751**, 77510F (2010).
8. K. Bartschat and M. J. Kushner, Proc. Natl. Acad. Sci. USA **113**, 7026 (2016).
9. A. H. Markosyan and M. J. Kushner, J. Appl. Phys. **120**, 193105 (2016).
10. O. Zatsarinny, K. Bartschat, N. Y. Babaeva, and M. J. Kushner, Plasma Sources Sci. Technol. **23**, 035011 (2014).
11. B. D. Barmashenko and S. Rosenwaks, J. Opt. Soc. Am. B **30**, 1118 (2013).
12. B. D. Barmashenko and S. Rosenwaks, Appl. Phys. Lett. **102**, 141108 (2013).
13. B. D. Barmashenko, S. Rosenwaks, and M. C. Heaven, Opt. Commun. **292**, 123 (2013).
14. A. M. Lietz and M. J. Kushner, J. Phys. D **49**, 425204 (2016).
15. A. H. Markosyan, A. Luque, F. J. Gordillo-Vázquez, and U. Ebert, Comput. Phys. Commun. **185**, 2697 (2014).
16. A. H. Markosyan, A. Luque, F. J. Gordillo-Vázquez, and U. Ebert, PumpKin: a tool to find principal pathways in plasma chemical models, 2014, http://www.pumpkin-tool.org.
17. Z. J. Jabbour, R. K. Namiotka, J. Huennekens, M. Allegrini, S. Milošević, and F. de Tomasi, Phys. Rev. A **54**, 1372 (1996).